united nations educational, scientific and cultural organization

international atomic energy agency

the
abdus salam
international centre for theoretical physics

SMR 1216 - 15

Joint INFM - the Abdus Salam ICTP School on
"Magnetic Properties of Condensed Matter Investigated by Neutron Scattering and Synchrotron Radiation Techniques"

1 - 11 February 2000

AN INTRODUCTION TO PHOTOEMISSION FROM MAGNETIC SYSTEMS

C. CARBONE
Forschungzentrum Jülich GmbH
Institut für Festkorperforschung
Postfach 1913, 52425 Jülich, Germany

An introduction to photoemission from magnetic systems

Notes for the ICTP School Trieste 2000

C. Carbone and L. Baumgarten

I. Introduction.

These notes describe the application of photoemission spectroscopy to the experimental investigation of magnetic systems. Photoemission is based on the photoelectric effects, discovered by Hertz in 1887 [1] and explained by Einstein in 1905 [2]. The absorption of a light quantum increases the energy of an electron by an amount $h\nu$, where frequency ν is the frequency of the light. If the acquired energy is sufficient to overcome the electron binding energy and the work function of the metal the electron can escape from the solid. The kinetic energy of the photoemitted electron can accordingly be written as :

$$E_{kin} = h\nu - E_B - \phi \qquad (I.1)$$

with E_B the electron binding energy referred to the Fermi energy and ϕ the work function. This relation describes the energy conservation in the photoemission process. It implies the quantum character of the radiation (a photon is either fully adsorbed or it is not adsorbed at all). Eq.(I.1) also shows that the electron binding energy in a solid can be determined by

measuring the kinetic energy of the photoemitted electrons, if the photon energy and the work function of the solid are known. Together with the relations that account for the momentum conservation Eq.(I.1) permits to determine the electronic band structure of solids from a photoemission experiment.

These manuscript gives an introduction to the study of the electronic bandstructure of magnetic materials with photoemission. The electronic structure constitutes a basis for the microscopic description of magnetism, as well as of most material properties. Although the basic elements of band theory were formulated already in 1920-1940, for a long time only limited experimental information was available on the bandstructure of solids. Insights on the electronic structure near the Fermi level were provided by electrical conduction, specific heat, and de Haas van Alphen measurements. X-ray emission and, since the sixties, photoemission [3] gave information on the density of states. The introduction of methods based on angle-resolved photoemission [4-7] and their refinement made possible in the last twenty years the detailed experimental investigation of band dispersion in solids. Also, the development of spin-resolved photoemission, pioneered in the late sixties [8], gave direct access to the spin-polarization effects in the electronic structure of ferromagnetic materials. Nowadays, intense synchrotron radiation allows to perform routinely photoemission measurements with the simultaneous analysis of the electron energy, emission angle, and spin polarization [9-10]. The energy dispersion relation as a function of wavevector and spin orientation ($E_B=E_B(\mathbf{k},\sigma)$), that fully describes the electronic structure of a ferromagnet in the limit of a non-relativistic and single-particle description, can be determined in this way. Moreover, the control of the light polarization provided by modern synchrotron radiation sources makes it possible to exploit dichroic effects in valence band and core-levels photoemission to probe the orientation of the magnetic moments and the symmetry of the electronic states [11].

II Bandstructure studies with Photoemission

II.1 Basic aspects of the method

Photoemission is a single-step process in which an electron is excited from its ground state in the solid into a final state in the vacuum. The theoretical description of the photoemission process in its general form is based on the „one-step-model", where the electron is excited from a Bloch state in the crystal into a damped final state near the surface. In the „three-step-model" the coherent photoemission process is instead divided into three incoherent parts that can be treated in a simpler way. This approximation turns out to be useful in many cases and it usually constitutes the first Ansatz in the interpretation of photoemission results. The three single steps are: (a) the absorption of a photon inside the solid, (b) the transport of the excited electron to the surface, and (c) the transmission of the electron though the surface into the vacuum. Each step is treated separately and the whole process is described as the product of the three single steps. In the following, the three-step model is described in its simplest form, the single particle approximation with free-electron final states:

(a) The electron excitation in the solid: The probabilty of an electronic transition from an initial state $|i\rangle$ into a final state $|f\rangle$ due to the absorption of a photon can be derived from first order perturbation theory. According to the "Fermi golden rule" :

$$W \propto \langle f|H'|i\rangle^2 \; \delta\left(E_f - E_i - h\nu\right) \qquad \text{(II.1)}$$

Substituting the electron momentum operator $\mathbf{P}$ of the unperturbed Hamilton operator by $\mathbf{P}+(e/c)\,\mathbf{A}$, one obtains the pertubation operator:

$$H' = \frac{e}{2mc}(\mathbf{A}\cdot\mathbf{P} + \mathbf{P}\cdot\mathbf{A}) + \frac{e^2}{2mc^2}|\mathbf{A}|^2 - e\Phi \qquad \text{(II.2)}$$

where $\mathbf{A}$ is the vector potential and $\Phi$the scalar potential of the incident radiation. The scalar potential Φ vanishes with a proper choice of the reference. Neglecting the term in $\mathbf{A}^2$ and using the commutation relation $[\mathbf{A},\mathbf{P}] = -i\hbar\nabla\mathbf{A}$ one obtains in the first order for the transition probability:

$$W \propto \left|\langle f|2\mathbf{A}\cdot\mathbf{P} - i\hbar\overline{\nabla}\cdot\mathbf{A}|i\rangle\right|^2 \delta(E_f - E_i - h\nu) \qquad \text{(II. 3)}$$

where $|i\rangle$ and $|f\rangle$ are wavefunctions of the unperturbed Hamiltonian. The δ function guarantees the energy conservation, ensuring that initial and the final state energy differs by hν. This relation must be distinguished from Eq.(I.1), as the former refers to the electron that has not left the solid yet. The matrix element can be further simplified setting $\overline{\nabla}\cdot\mathbf{A} = 0$, a condition fulfilled for a transversal wave fields. Longitudinal field components can appear near the surface and are often important near the plasmon excitation. For photon energy well above the plasmon energy their effect ("surface photo-effect") can be generally neglected. The photoelectron trasition probability can then be written in the usual form:

(II.4a) $$W \propto \left|\langle f|\mathbf{A}\cdot\mathbf{P}|i\rangle\right|^2 \delta(E_f - E_i - h\nu)$$

Two other relations can be derived from the commutation relation of H_o with P and r:

(II.4b) $$W \propto \left|\langle f|\mathbf{r}|i\rangle\cdot\mathbf{A}\right|^2 \delta(E_f - E_i - h\nu)$$

$$W \propto \left|\langle f|\bar{\nabla}V|i\rangle\cdot\mathbf{A}\right|^2 \delta(E_f - E_i - h\nu)$$

A second conservation rule requires the momentum to be conserved in the photoexcitation. The photon momentum is negligible in comparison to the electron momentum for photon energy below 1 keV. Since energy and momentum conservation can not simultaneously be fulfilled, a free electron cannot absorb a photon (Fig.1a). Fig.1b represents the photoexcitation in a solid, with the bandstructure schematically described as a nearly-free-electron band. In a solid the additional momentum to fulfill energy and momentum conservation is provided by a reciprocal lattice vector **G**, so that:

(II.5) $$\mathbf{k}_f = \mathbf{k}_i \pm \mathbf{G}$$

where $\mathbf{k}_i$ is the initial state wave vector and $\mathbf{k}_f$ the final state wave vector.

Fig.1b and Eq.(II.5) show that there exist an univoque relation between the final and the initial state momentum. The momentum of the initial state is therefore determined if the momentum in the final state is known. Moreover, transitions from different initial states can be selected by varying the photon energy. As it will be shown in the following, it is possible to probe the complete bandstructure by properly choosing the photon energy and the experimental geometry .

(b) The transport of the photoelectron in the solid - A direct relation between the energy and momentum of the electrons detected outside the crystal and those quantities inside the crystal can be established only if the electron does not loose energy on its way to the surface. Inelastically scattered electrons are practically lost for the band structure determination. The occurrence of a cascade of inelastic scattering processes produces a large number of low energy electrons. In the photoemission spectra these so-called secondary electrons give rise to a nearly structureless background with a large peak at very low kinetic energy (Fig.2) [12]. The scattering processes determine the mean free path of the electrons and therefore the probing depth of photoelectron spectroscopy. The electron mean free path depends on the material and on the electron energy, as shown in Fig.3 [13]. It is shortest in an energy range around 50 eV. This is an importat energy region for photoelectron spectroscopy. The information depth corresponds here to only a few atomic layers and this makes photoemission a very surface sensitive method. This is of advantage for the study of surface processes, as for example adsorption and catalytic reactions, and of very thin film properties. On the other hand, the interpretation of photoemission spectra (even for high electron kinetic energy of 1-2 keV) has always to take into account the influence of surface effects (e.g. surface electronic structure, chemical composition, and contamination). An example is the often prominent spectral contribution from surface states, i.e. electronic states that are localized at the surface, that will be discussed in a following paragraph.

(c) The escape through the surface - Refraction effects occur as the electron passes from the solid to the vacuum. Schematically these are shown in Fig.4. They are caused by the potential change at the surface, breaking the symmetry of the system in direction normal to the surface plane. As a consequence, the component of the momentum perpendicular to the surface is not conserved as the electron leaves the solid. The parallel component of the electron momentum

remains unchanged, since the symmetry of the system parallel to the surface is preserved. The momentum components outside the crystal are simply obtained considering the quadratic dependence of the kinetic energy on the total momentum :

$$\mathbf{p}_{//} = \mathbf{p} \cdot \sin\theta = \frac{\sqrt{2m}}{\hbar}\sqrt{E_{kin}}\sin\theta \qquad \text{(II.6)}$$

$$\mathbf{p}_{\perp} = \mathbf{p} \cdot \cos\theta = \frac{\sqrt{2m}}{\hbar}\sqrt{E_{kin}}\cos\theta$$

where θ is the emission angle with respect to the surface normal.

To determine the bandstruture of the solid, the components of the wave vector inside the solid have to be traced back from these values. This is simple for the parallel component ($\mathbf{p}_{//} = \mathbf{k}_{//}(\pm\mathbf{G})$). The scheme in Fig.4 helps to find the relation between the perpendicular component of the moment inside and outside the solid. The kinetic energy outside the crystal has zero value at the vacuum level, defined by the crystal workfunction. Inside the crystal the zero point of the energy parabola is the lowest edge of the conduction band. The potential change at the surface, i.e. the potential difference between the two parabolas, is the inner potential V_0. The electron kinetic energy can accordingly be written either as function of the wavevector k inside the crystal or as a function of the momentum component p outside the crystal :

$$E_{kin} = \frac{\hbar^2 k_{//}}{2m} + \frac{\hbar^2 k_{\perp}^{\,2}}{2m} - V_0 = \frac{\hbar^2 p_{//}^{\,2}}{2m} + \frac{\hbar^2 p_{\perp}^{\,2}}{2m} = E_{kin}\sin^2\theta + E_{kin}\cos^2\theta \qquad \text{(II.7)}$$

Considering the conservation of the parallel component:

$$k_{//} = \frac{\sqrt{2m}}{\hbar}\sqrt{E_{kin}}\sin\theta \qquad \text{(II.8)}$$

$$k_{\perp} = \frac{\sqrt{2m}}{\hbar}\sqrt{E_{kin}\cos^2\theta + V_0}$$

Together with the relation for the energy conservation, (Eq.(I.1)) $E_{kin} = h\nu - E_B - \phi$, these formulas provides the basis for determining the bandstructure with angle-resolved photoemission. They permit to derive the binding energy and wave vector of a state inside the solid from the measurements of externally accessible quantities as the photoelectron kinetic energy and emission angle. In these equations appears yet an unknown parameter, the inner potential V_0. However, also this quantity can be experimentally determined. A detailed description of the so-called triangulation method is given by Hüfner [7]. A very simple method, although not fully independent from the theory, will be presented in the next paragraph.

It should be also noticed that only the relation betwen photoelectron energy and momentum is needed to determine the bandstructure. The complicated calculation of the matrix elements introduced above is not required to this purpose. In the intrepretation of the experimental data the influence of the matrix elements (Eq.(II.4)) is usually taken into account through simple symmetry considerations. Symmetry considerations („dipole selection rules") predict for some experimental geometries vanishing matrix elements for certain initial states. Essentially, selection rules allow to identify the symmetry of the states contributing to the spectra, by changing the measurement geometry or the light polarization [5-6].

II.2 *Band mapping*

Some aspects of the methods described above will be briefly illustrated in the following. The first example (a) considers the photoemission from a two-dimensional system. In this case the problem of determining the inner potential V_0 and the perpendicular wavevector component does not arise (i.e. $k_\perp$ is not a good quantum number). The second example (b) shows a simple method to determine the inner potential V_0 in a photoemission experiment on a three-dimensional system.

(a) In any three-dimensional systems there are states of two-dimensional character. These are the so-called surface and interface states. These states exist only in the proximity of the surface of a crystal or at the interface between two materials. They are special solutions of the Hamiltonian, allowed by the existence of a potential change at the suface (or interface), in regions of the bandstructure that are forbidden for the Bloch states of the three-dimensional crystal. The two-dimensional character of these states is clear, since their existence is restricted to the surface or interface region. Their band dispersion can be fully determined by measuring the photoelectron kinetic energy and the momentum component parallel to the surface.

Fig.5a shows the photoemission spectra of the best known surface states of the 3d-metals as a function of the emission angle [14]. This is a sp-derived state near the Fermi energy at the Cu(111) surface. The binding energy is referred with the help of the Eq.(I.1) to the Fermi level. The parallel component of the wave vector can be determined for any emission angle from the electron kinetic energy according to Eq.(II.8). The bandstructure of the surface state is obtained by plotting the binding energy as a function of the wavevector ($E_B = E_B(\mathbf{k}_{//})$). This

is shown in Fig.5b. The surface state has a parabolic dispersion, with a binding energy maximum of 390 meV. Its dispersion can be described as $E_B(eV)= 8.52[eV/A^{-2}]\ k_{//}^2\ [A^{-2}]$ - 0.39 [eV]. In Fig.5b the shadowed area shows the regions where there exist three-dimensional bulk states. The surface states lays, as expected, in a bandgap. Another example of photoemission from states of two-dimensional character, for Cu films on Co(100), will be discussed in the next chapter (III.3).

(b) For a three dimensional system the problem of determining the perpendicular component of the wavevector (Eq.(II.8)) (i.e. the unknown inner potential V_0) arises. In order to determine V_0, it is sufficient to know the perpendicular wavevector component corresponding to just one value of the perpendicular momentum outside the crystal. When V_0 is known all other wave vector can be simply derived (Eq.(II.8)). A simple way to determine V_0 is described in the following. Fig.6a shows the Brillouin zone of a face centered cubic crystal, the three low-index directions of the real lattice and the labels of various symmetry points in the reciprocal space. Fig.6b shows the relation between wave vector, photon energy, and emission angle from the (100) surface. This plot assume that the parallel component of the wave vector lays in (100) direction. In this geometry, for a fixed binding energy, changing the emission angle probe the initial states along a circle in the Γ-X-W-K plane. In normal emission, varying only the photon energy, the wave vector periodically crosses the Γ and the X point. This periodicity appears also in the photoemission spectra. The dispersion of the states is symmetric with respect to T and X and has therefore to display a (local) energy extreme at these points. Such extremal binding energy values are easily found in series of spectra measured as a function of the photon energy. Fig.7a shows fcc-Co(100) spectra, measured with a light polarization that (according to the dipole selection rules) excites the Δ_5

bands. The spectra display a dispersive feature that reaches its maximum binding energy near 46.5 eV. In order to associate this extremal value to either the Γ or X symmetry point, the band structure has to be known only very approximatively. Fig.7b displays a theoretical band structure of Co [15]. A comparison of the binding energies and the cosideration of the dipole selection rules shows that the observed binding energy maximum derives from the Γ-point. In this way one wave vector is determined and V_0 is therefore known. The dispersion of the initial state bands ($E_B=E_B(\mathbf{k})$) along the Γ - X direction can be traced back from the spectra according to the Eq.(II.7) and Eq.(II.8), that associate the wave vector to the electron kinetic energy and emission angle. In off-normal geometry, simple trigonometry considerations generalize this approach. As shown in Fig.6a initial states at various symmetry point can be examined by varying emission angle and photon energy.

III Photoemission from magnetic systems

III.1 Spin-dependent bandstructure

In ferromagnetic solid the spin degeneracy of the electronic bands is lifted by the exchange interaction. Electrons with different spin orientation have thus a different band structure. The natural quantization axis for the electron spin is the macroscopic magnetization direction. Electrons with spin moment parallel to the magnetization direction are defined as majority-spin electrons and electrons with opposite spin moment orientation as minority-spin electrons. Since the Fermi energy is the same for the two spin-orientations, lifting the spin degeneracy leads to an unequal occupation of majority- a minority-spin bands, and thus to a magnetic

The above presentation has made use of a very simple a suggestive picture based on a single particle description of the photoemission process. This model, although certainly oversimpified, is often sufficient to provide a consistent and rather accurate description of the valence band spectra. However, the shortcoming of this approximation become evident in those systems with more correlated electrons. In Fe and Co, for example, the single particle picture gives a quite reasonable basis for the data analysis, as shown above (Fig.10), but correlation effects need to be considered for a quantitative description. Formally it can be shown that the photoemission intensity distribution is proportional to the quasi-particle spectral density function, which only in the limit of vanishing correlations reflects the one-particle band dispersion. In Ni, for example, the splitting between majority- and minority-spin states in the photoemission spectra is systematically smaller than the calculated exchange splitting. This discrepancy, as well as the presence of satellite structures in the valence spectra, is well understood in the theoretical frames that include correlation effects and multielectron excitations. It has also to be mentioned here that a single particle picture completely fails to describe the photoemission from the localized and highly correlated 4f electrons in magnetic rare earth systems.

III.2 Electronic properties and magnetism

A main aim of photoemission experiments on magnetic systems is to examine the corrrelation between the magnetic properties and the electronic structure. In this paragraph, a few examples illustrate photoemission investigations on the relation between the electronic structure and (a) the magnetization at finite temperature, (b) temperature and transport properties (CMR), (c) finite size and interlayer coupling.

(a) Finite Temperature effects - The relation between electronic and magnetic properties at finite temperature is a central question for many branches of solid state physics. While electronic theory accurately accounts for the ground state properties of magnetic materials, it meets only limited success in describing the finite temperature behaviour, such as magnetic phase transitions, the corresponding ordering temperatures, and the critical parameters. The simplest model describing the finite temperature behaviour of the electronic structure is the Stoner model. In the Stoner model the reduction of the exchange splitting at finite temperature simply parallels the corresponding changes of the macroscopic magnetization. To what extent this picture can be applied to describe the finite temperature behaviour in a real case is still an open issue. It is generally assumed that the Stoner model can reasonably describe the most delocalized states, while the splitting of strongly localized states remains unchanged due to the local exchange interaction, even in magnetically disordered systems.

The temperature dependence of the photoemision spectra can directly probe the changes of the electronic structure at finite temperature. The 3d states of itinerant ferromagnetic systems (as Fe, Co, and Ni) present a complicated finite temperature behaviour, which is intermediate between the two extreme cases and also depends on the character of the specific electronic state [18-19]. A simple case that illustrates how photoemission can be used to follow the temperature-induced change of the ferromagnetic bandstructure is represented by the (5d6s)-states of Gd. The (5d6s)-valence states in Gd are extended states that mediate the ferromagnetic coupling through the large 4f Gd moments. These states display a behaviour at finite temperature that closely follows the simple Stoner model [20-21]. Fig.11a shows the photoemission spectra from the Gd (5d6s) bands as a function of temperature. A pair of exchange-split bulk states is observed at 2.4 and 1.5 eV binding energy, while a surface state gives rise to an intense peak near e Fermi energy. With increasing temperature, the exchange

splitting of the bulk states decreases, in a way that closely corresponds to the reduction of the overall magnetization (Fig.11b). At the Curie temperature the exchange splitting cannot anymore be detected in the spectra, indicating that it is quite small or even vanished (as assumed in the Stonel model). The experimental indications of a Stoner behaviour for the bulk Gd valence states appears to be related to their significantly more delocalized character in comparison to the 3d transition metal wavefunctions and also to the 4f-states in Gd itself. Similarly, it is conceivable that the temperature behaviour varies to a certain extent within the Gd valence band, depending on the degree of itineracy of the different electronic states. Noteworthy, there are theoretical and experimental evidences indicating that the more strongly localized surface states (near the Fermi energy in Fig.13) have a significant exchange splitting also above the bulk Curie temperature.

(b) temperature and electrical transport - Magneto-electronics is an emerging field in magnetism with important connections to applications. It consists of various phenomena where a change of the magnetic state of the system has a directly influence on its transport properties. Photoemission experiments can adress the microscopic relation between electronic and magnetic properties. Important classes of materials for magneto-electronics are those displaying the CMR ("colossal-magneto-resistance") and GMR ("giant-magneto-resistance") effect. The first case considered here is the electronic structure of ferromagnetic $La_{0.7}Sr_{0.3}MnO$ films, a manganese perovskite with 'colossal" negative magnetoresistance [22]. The largest magnetoresistance effect occurs near the Curie temperature upon crossing the paramagnetic-ferromagnetic transition. Also, associated to the magnetic transition is a large decrease of the resistivity. The understanding of the microscopic mechanisms that determine the transport

properties of these systems is presently of great interest, also for the potential technical application of these oxide materials.

The photoemission spectra of the films (Fig.12, left) give evidence of a change in the electronic structure acrosss the transition temperature: the spectrum shows a negligible intensity at the Fermi level above the Curie temperature, whereas it clearly displays a metallic Fermi level cut-off below the Curie temperature [23]. This temperature dependence is peculiar to the doped manganese perovskite. It turns out to be also associate to a particular character of the conduction electronic states in the ferromagnetic phase. Fig.12 (right) shows the spectra of the films below the Curie temperature measured with analysis of the photoelectron polarization. The most striking observation is that the emission at the Fermi energy consists of majority-spin electrons only. In contrast, the minority-spin spectral intensity disappears near E_F [37]. This observation demostrates that the manganese perovskite in its ferromagnetic state is an half-metallic-material. Half-metallic ferromagnets are materials with metallic character for the majority spin states and an insulating one for the minority-spin states. In $La_{0.7}Sr_{0.3}MnO$ the majority-spin states show a metallic character (with states at E_F) with charge carriers from the Mn 3d states. The minority-spin states exhibit an insulating gap between the occupied O 2p states and the unoccupied Mn 3d minority spin-states. Above the Curie temperature the Mn spin moments become disordered and the spin-anisotropy disappears (see Fig.13). The existence of half-metallic materials was previously predicted [24] but it was not proven before. Since half-metallic ferromagnet have 100% polarization for the electronic states at the Fermi energy, they are best candidates for obtaining high spin-polarized currents. This makes them obviously attractive for technologial applications that exploits the spin-dependent transport of polarized electrons.

(c) Finite size effects and interlayer coupling - An other class of systems where transport and magnetic properties are closely connected is constituted by magnetic multilayers. An oscillatory interlayer coupling was discovered in Fe/Cr multilayers in 1986 [25]. Light scattering measurements gave evidence that two thin Fe layers are antiferromagnetically coupled when they are separated by a thin (~ 10 Å) non-magnetic Cr layer. The antiferromagnetic alignment of the film magnetization results from an indirect and long range magnetic interaction mediated by the non-magnetic (spacer) layer. Later investigations established that this indirect coupling is a quite general property of multilayers, exhibited by several combinations of film materials. The interaction has an oscillatory form as a function of the spacer thickness and, therefore, of the separation between the magnetic films [26]. The interlayer coupling changes sign in a periodic way as a function of the thickness of the non-magnetic layer (Fig.14a). It gives alternately rise to ferromagnetic and antiferromagnetic alignment of the film magnetization. The interaction is defined by one or more superimposed periods, which are characteristic of the non-magnetic spacer material and its crystallographic orientation. Film structures with antiparallel magnetic coupling display remarkable changes of electrical resistance in an external magnetic field (GMR effect) [27]. The resistance has maximum value in field-free condition and decreases with increasing field (Fig.14b). It reaches a minimum when the field is sufficiently large to overcome the interlayer coupling and it alignes the magnetization of all films.

Theories based on the RKKY interaction scheme relate the oscillatory behaviour of the coupling and its characteristic periods to the topology of the Fermi surface of the non-magnetic space. The coupling periods correspond to inverse of the reciprocal space vectors spanning stationary points of the Fermi surface [28]. For example, the two oscillation periods (2.6 and 5.9 atomic layers) of the interlayer coupling through Cu(100) films correspond to the

reciprocal vectors indicated in Fig.15. A detailed understanding of the coupling has been developed as theoretical [29] and experimental studies [30-33] drew attention to finite size effects on the film electronic structure. The oscillatory coupling turns out to originate from the electron confinement in the thin spacer layers. The coupling is due to specific electronic states of the films that, for analogy with the confined states in a quantum well potential, are called „quantum welll states".

The fundamental difference between the two-dimensional electronic structure of a film and the one of a three dimensional solid is due to the boundary conditions at the interfaces. In the ideal case of an isolated film composed of n layers, its finite size imposes a quantization of the levels, so that only n discrete levels $E_n=E_n(k_{//})$ exist for each two-dimensional vector $k_{//}$. The electronic structure of such a film (in this ideal limit) has a two-dimensional character, as the the surface states in par. IIb. The spectrum of the energy levels depends on the film thickness as schematically indicated in Fig. 16a, in analogy with the simple case of a particle in a potential well. The number of states in the film increases proportionally with the film thickness (represented in the analogy by the width of the potential well). For a (non-isolated) film on a substrate, or part of a multilayer, the electron transmission and reflection at the interfaces determine the degree of confinement of the electron wave functions. Strongly reflected electron waves remain confined within the film and form „quantum well states".

Fig.16b shows normal emission spectra of epitaxial Cu films on fcc-Co(100)[32]. Photoemission probes in this geometry states of Δ_1 symmetry and wave vector $k_{//} = \Gamma$, that are related by the RKKY models to the long (5.9 monolayer) coupling period [22, 28] (Fig. 15b). The spectra show several structures due to quantum well states, with binding energy varying as a function of the Cu film thickness. Fig.17a compares the photoemission results with calculated binding energy of "quantum well states". Experimental and calculated quantum

well energies lie on a number of well distinct curves. A new state reaches the Fermi level at regular intervals of about 6 atomic layers, that correspond to the long period of the oscillatory coupling through Cu(100) layers. As a function of film thickness, the „quantum well states" induce thus at the Fermi energy a modulation of the density of states with this period.

The photoemission intensity at the Fermi level directly displays this oscillatory behaviour (Fig.17b). A maximum appears as a quantum well state reaches the Fermi energy, while a minimum occurs as with increasing thickness the state moves away from it. Also, the modulation of the density of states due „quantum well states" can be examined in any other point of the reciprocal space by varying the photoelectron collection angle [33,34]. Fig.17b shows also the fast oscillatory behaviour of the photoemission intensity near the Fermi energy for the wave vector $k_{//}$ associated to the short-period (about 2.6 monolayers) oscillation [34].

Photoemission with spin-polarization analysis demonstrates that these „quantum well states" in the Cu film have a predominant minority-spin character. Fig.18a displays the Cu quantum well spectra decomposed in the two spin components. The „quantum well states" appear as prominent structures in the minority-spin channel, whereas they are weak (or absent) in the majority-spin spectra. This can be easily understood since the Co substrate acts as a spin-dependent potential barrier for the confinement of the electronic wave function (Fig.18b). The electron wave functions are reflected at the interface to a degree that depends on their spin character. The minority-spin electrons, for which the potential is very different in the two metals, are strongly reflected at the interface and remain therefore confined in the Cu film. Conversely, the majority spin electrons, which have in the two metals similar energy, are weakly reflected and become delocalized over the two materials. The electronic structure of paramagnetic Cu films in contact with the ferromagnetic substrate acquires in this way a magnetic character, i.e. a dependence on the electron spin orientation.

Fig.19 illustrates schematically how quantum well states give rise to the indirect exchange coupling. The potentials for electrons of opposite spin character are indicated for two magnetic films separated by a non-magnetic layer. The confinement of the electronic wave functions depends on the relative orientation of the film magnetization. The electrons remain strongly confined within the spacer into the (spin-down) „quantum well states" only if the magnetization of the ferromagnetic films is parallel. The total energy of the (parallel or antiparallel) magnetic configuration has an oscillatory behaviour reflecting the crossing of states through the Fermi level. Every time a quantum well level crosses the Fermi level the energy the system gains or looses energy in filling the new state, favouring alternatively the configuration with parallalel or antiparallel magnetization. The oscillatory interlayer coupling is thus connected to the modulation of the density of states at the Fermi level due to spin-polarized „quantum well states". The period, the amplitude, and the phase of the modulation that the „quantum well states" induce on the density of states at E_F, correspond to the period, the strength and the phase of the oscillatory coupling. The "quantum well states" manifest themself also in other magnetic phenomena as in the oscillatory behaviour of the film anisotropy, the modulation of the linear Kerr effect and of the second harmonic generation. Furthermore, recent theoretical work shows that quantum well states contribute directly in a significant way to the electrical resistance changes (GMR) in multilayers.

IV Appendix. Electron Analyzers

The essential experimental requirements for angle-resolved photoemission are defined by Eq.II.8. The measurement has to determine the electron kinetic energy as a function of the

emission angle. Modern electron spectrometers consist typically of three main parts: an energy dispersive element that measures the electron kinetic energy; an electrostatic electron lens, that select the emisison angle, and transmit and focus the electrons on the entrance slits of the dispersive element; and an electron detector. Fig.20 shows a scheme of a typycal energy analyzer [35]. The energy dispersive element consists of two half-spheres, across which a potential difference is set. The half-spheres simulate the electrostatic potential of a point charge in the center of a sphere. Between the half-spheres the electrons describe a Kepler orbit, with a radius defined by the potential difference between the spheres and by the electron kinetic energy. As the analyzer slits define two foci, in the entrance and exit plane, only electrons with a certain energy (the pass energy) can pass through the analyzer. Varying this energy (either by changing the potential between the spheres, or the potential between the sample and the analyzer) the number of photoemitted electron can be determined as a function of their kinetic energy. The electron detectors are usually simple electron multipliers or two-dimensional multichannel plates. The use of a multichannel plate allows to exploit the linear energy dispersion of a spherical analyzer. If the analyzer is operated without an exit slit, parallel dectection of electrons of different kinetic energy can be obtained with a position sensive multichannel plate in the exit plane of the analyzer.

Additional information on the electronic structure of a ferromagnetic system can be obtained measuring in addition the spin-polarization of the photoemitted electrons. In a spin-polarized photoemission experiment, an eletron energy analyzer is combined with a spin-detector. All spin-detectors used until now in electron spectroscopy for measuring the spin polarization rely on the spin-dependent scattering from a solid target. The spin-analyzers can be divided, according to the energy of the scattered electron beam, between low-energy (~ 10 eV - 1 keV) and high energy (up to 100 keV) methods. An examples of low energy methods is

the LEED detector [36], where an electron beam is diffracted by a W single crystal, and the reflected beam detector [37], exploiting the spin-dependent reflection of the electrons at the Fe/vacuum interface. The so-called Mott detectors are typical high energy polarimeter that rely on spin-orbit effects in the scattering from heavy nuclei [38]. They are the most commonly used electron spin analyzers. No effective method for the analysis of the electron spin polarization is yet available, in contrast, for example, with the high efficiency of light polarizing filters. The spin-analysis involves a counting rate loss of the order of 10^{-4} with respect to a conventional photoemission experiment. High photon flux sources, as synchrotron radiation (in particular from insertion-device), are thus generally required in a spin-resolved photoemission experiment to compensate for the low efficiency of the spin polarimeters.

Fig.21 shows schematically the experimental set-up of a spin-resolved photoemission experiment with a Mott polarimeter. The orientation of the photoelectron spins (i.e. the spin polarization of the photoelectron beam) is then determined with a Mott polarimenter, located behind the exit slits of the energy analyzer. The electron beam is accelerated behind the exit slits of the energy analyzer to high energy (10 keV - 100 keV). The beam is then scattered by a thin Au foil, of typically about 1000 Å thickness. The spin-orbit interaction with the Au nuclei produces a left-right asymmetry of the backwards scattered beam intensity, that is measured by a pair of detectors symmetrically placed with respect to the normal to the foil. The measured asymmetry is conveniently defined as :

$$A_z(E_{kin}) = \frac{N_l(E_{kin}) - N_r(E_{kin})}{N_l(E_{kin}) + N_r(E_{kin})} \qquad \text{(IV.1)}$$

where $N_l(E_{kin})$ and $N_r(E_{kin})$ are the electrons counted by the left and right detector, respectively, as function of the electron energy. This asymmetry is proportional to the

component of the spin polarization, P_z, perpendicular to the scattering plane. The geometry of the experiment can be conveniently chosen so that the z direction is parallel to the sample magnetization, therefore:

$$P_z(E_k) = \frac{N_\uparrow(E_{kin}) - N_\downarrow(E_{kin})}{N_\uparrow(E_{kin}) + N_\downarrow(E_{kin})} \qquad \text{(IV.2)}$$

where $N_\uparrow(E_{kin})$ and $N_\downarrow(E_{kin})$ are the number of photoelectrons with spin moment parallel and antiparallel to the magnetization direction, respectively. The proportionality relation between measured asymmetry A and P_z is simply given by :

$$P_z = \frac{A_z}{S} \qquad \text{(IV.3)}$$

where S, the Sherman function, is a (known) characteristic parameter of the experimental set-up (e.g., geometry, foil thickness, beam energy). Together with the above relation, the equation:

$$N(E_{kin}) = N_l(E_{kin}) + N_r(E_{kin}) = N_\uparrow(E_{kin}) + N_\downarrow(E_{kin}) \qquad \text{(IV.4)}$$

allows to determine the spin-resolved photoemission spectra $N_\uparrow(E_{kin})$ and $N_\downarrow(E_{kin})$. The spin-resolved photoemission spectra reflect the different energy and occupancy of states with opposite spin character in a magnetic material (Fig. 3), which is, in fact, the microscopic cause of ferromagnetism.

References

[1] Hertz, Ann. Physik **31,** 983 (1887).

[2] A. Einstein, Ann. Physik **17**, 132 (1905).

[3] K.Siegbahn, C.Nordling, R. Fahlman, R. Nordberg, K. Hamrin, J. Hedman, G. Johansson, T. Bergmark, S.-E. Karlsonn, I. Lindgren, B. Lindberg, "ESCA, Atomic, Molecular and Solid State Structure Studies by means of Electron Spectroscopy" Nova Acta Regiae Soc. Sci., Upsaliensis, Ser. IV, Vol. 20 (1967); C.N. Berglund and W.E. Spicer, Phys. Rev. **136**, A 1030 (1964).

[4] E.W. Plummer and W. Eberhardt, Advances in Chemical Physics **49**, 533, John Wiley & Sons (New York) 1982.

[5] F.J. Himpsel, Advances in Physics **32**, 1 (1983).

[6] S.D. Kevan, ed., „Angle-Resolved Photoemission" Elsevier (Amsterdam) 1992.

[7] Hüfner, „Photoelectron spectroscopy", Springer Series in Solid Sate Science 82, Springer-Verlag Berlin Heidelberg New York, (1996).

[8] H.C. Siegmann, Phys. Rep. C **17**, 38 (1975); S. F. Alvarado, W. Eib, F. Meier, H. C. Siegmann, D. Zürcher, in "Photoemission and Electronic Properties of Surfaces, ed. B. Feuerbacher, B. Fitton, R. F. Willis, Wiley (New York), 1978.

[9] E. Kisker and C. Carbone, *"Angle Resolved Photoemission"*, ed. S.D. Kevan, Elsevier (Amsterdam) 1992.

[10] P.D. Johnson, Rep. Prog. Phys. **60**, 1217 (1997).

[11] L. Baumgarten, C. M. Schneider, H. Petersen, F. Schäfer, J. Kirschner, Phys. Rev. Lett. **23**, 492 (1980); W. Kuch, A. Dittschar, K. Meinel, M. Zharnikov, C.M. Schneider, J.

Kirschner, R. Feder, Phys. Rev. B **53**, 11621 (1996); Ch. Roth, F.U. Hillebrecht, H. Rose, E. Kisker, Phys. Rev. Lett. **70**, 3479 (1993).

[12] W.Eberhardt , Doktorarbeit, Universität Hamburg (1978).

[13] A. Zangwill, "Physics at surfaces", Cambridge University Press, Cambridge (1988).

[14] S.D. Kevan, Phys. Rev. Lett. **50**, 526 (1983).

[15] A. Fanelsa, E. Kisker, J. Henk, and R. Feder, Phys. Rev. B **54**, 2922 (1996).

[16] K.B. Hathaway, H.J.F., A.J. Freeman, Phys. Rev. B **31**,7603 (1985).

[17] W. Clemens, T. Kachel, O. Rader, E. Vescovo, S. Blügel, C. Carbone, W. Eberhardt, Sol. State Comm. **81**, 739 (1992); R. Kläsges, Doktorarbeit, Universität zu Köln (1998).

[18] E. Kisker, K. Schroder, M. Campagna, and W. Gudat, Phys. Rev. Lett. **52**, 2285 (1984).

[19] K.P. Kamper, W. Schmitt, G. Guntherodt, Phys. Rev. B **42**, 10596 (1990).

[20] B. Kim, A. B. Andrews, J. L. Erskine, K. J. Kim, B. N. Harmon, Phys. Rev. Lett. **68**, 1931 (1992).

[21] K. Maiti, C.M. Malagoli, A. Dallmeyer, and C. Carbone, to be published

[22] J.H. Park, E. Vescovo, H.J. Kim, C. Kwon, R. Ramesh, and T. Venkatesan,Nature, **392**, 794 (1998).

[23] R. Von Helmotz, J. Wecker, B. Holszapfel, L. Schultz, and K. Samwer, Phys. Rev. Lett. **71**, 2331 (1993).

[24] A. De Groot, F.M.Muller, P.G. van Engen, and K.H.J. Buschow, Phys. Rev. Lett. **50**, 2024 (1983).

[25] P. Grünberg, R. Schreiber, Y. Pang, M.B. Brodsky, and H. Sowers, Phys. Rev. Lett. **57**, 2442 (1986).

[26] S.S. Parkin, N. More, and K. P. Roche, Phys. Rev. Lett. **64**, 2304 (1990).

[27] M. N. Baibich, J. M. Broto, A. Fert, F. Nguyen Van Dau, F. Petroff, P. Etienne, G. Creuzet, A. Friederich, and J. Chazelas, Phys. Rev. Lett. **61**, 2472 (1988).

[22] P. Bruno and C. Chappert, Phys. Rev. Lett. **67**, 1602, 2592 (1991).

[28] M.D. Stiles, Phys. Rev. B **48**, 7238 (1993); L.Nordström, P. Lang, R. Zeller, and P.H. Dederichs, Europhys. Lett. **29**, 395 (1995).

[29] J. E. Ortega, and F.J. Himpsel, Phys. Rev. Lett. **69**, 844 (1992).

[30] K. Garrison, Y. Chang, and P.D. Johnson, Phys. Rev. Lett. **71**, 2801 (1993).

[31] C. Carbone, E. Vescovo, O. Rader, W. Gudat, W. Eberhardt,. Phys. Rev. Lett. **71**, 2805 (1993); C. Carbone, E. Vescovo, R. Kläsges, W. Eberhardt, Sol.State Comm. **100**, 749 (1996).

[33] D. Li, J. Pearson, S. Bader, E. Vescovo, D.-J. Huang, P.D. Johnson, B. Heinrich, Phys. Rev. Lett. 78, 1154 (1997); R.K. Kawakami, E. Rotenberg, E.J. Escorcia-Aparicio, Hyuk J. Choi, T.R. Cummins, J.G. Tobin, N.V. Smith, and Z.Q. Qiu, Phys. Rev. Lett. **80**, 1754 (1998); J.J. Paggel, T. Miller, T.C. Chiang, Phys. Rev. Lett. **81**, 5632 (1998).

[34] P. Segovia, E.G. Michel, J.E. Ortega, Phys. Rev. Lett **77**, 3455 (1996); R. Kläsges, D. Schmitz, C. Carbone, W. Eberhardt, P. Lang, R. Zeller, P.H. Dederichs, Phys. Rev. B, Phys. Rev. B **57**, R696 (1998).

[35] S.D. Kevan, Rev. Sci. Instrum. **54**, 1441 (1983).

[36] J. Kirschner and R. Feder, Phys. Rev. Lett. **42**, 1008 (1979).

[37] D. Tilmann, R. Thiel, and E. Kisker, Z. Phys. B **77**,1 (1989).

[38] J. Kessler, "Polarized Electrons", Springer (Berlin) (1976).

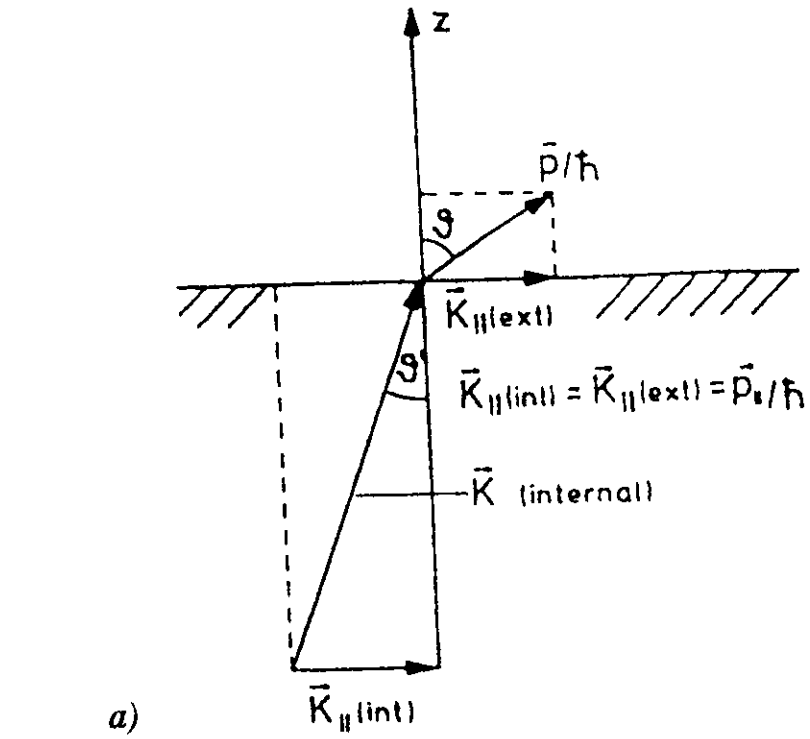

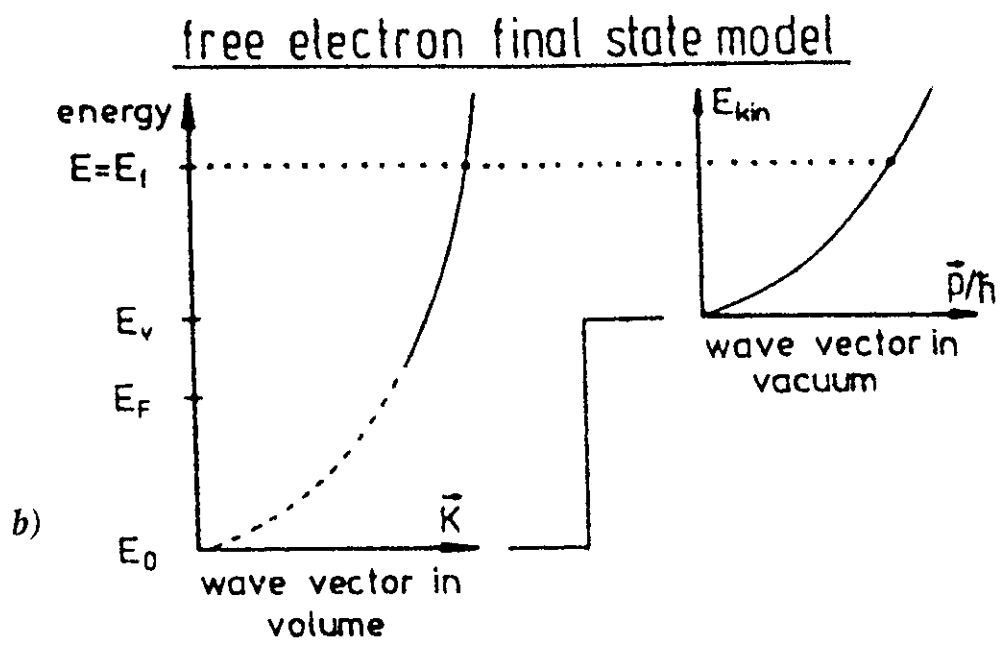

Fig. 4 a) Refraction and electron wave vector at the surface. b) Model of the inner potential V_0

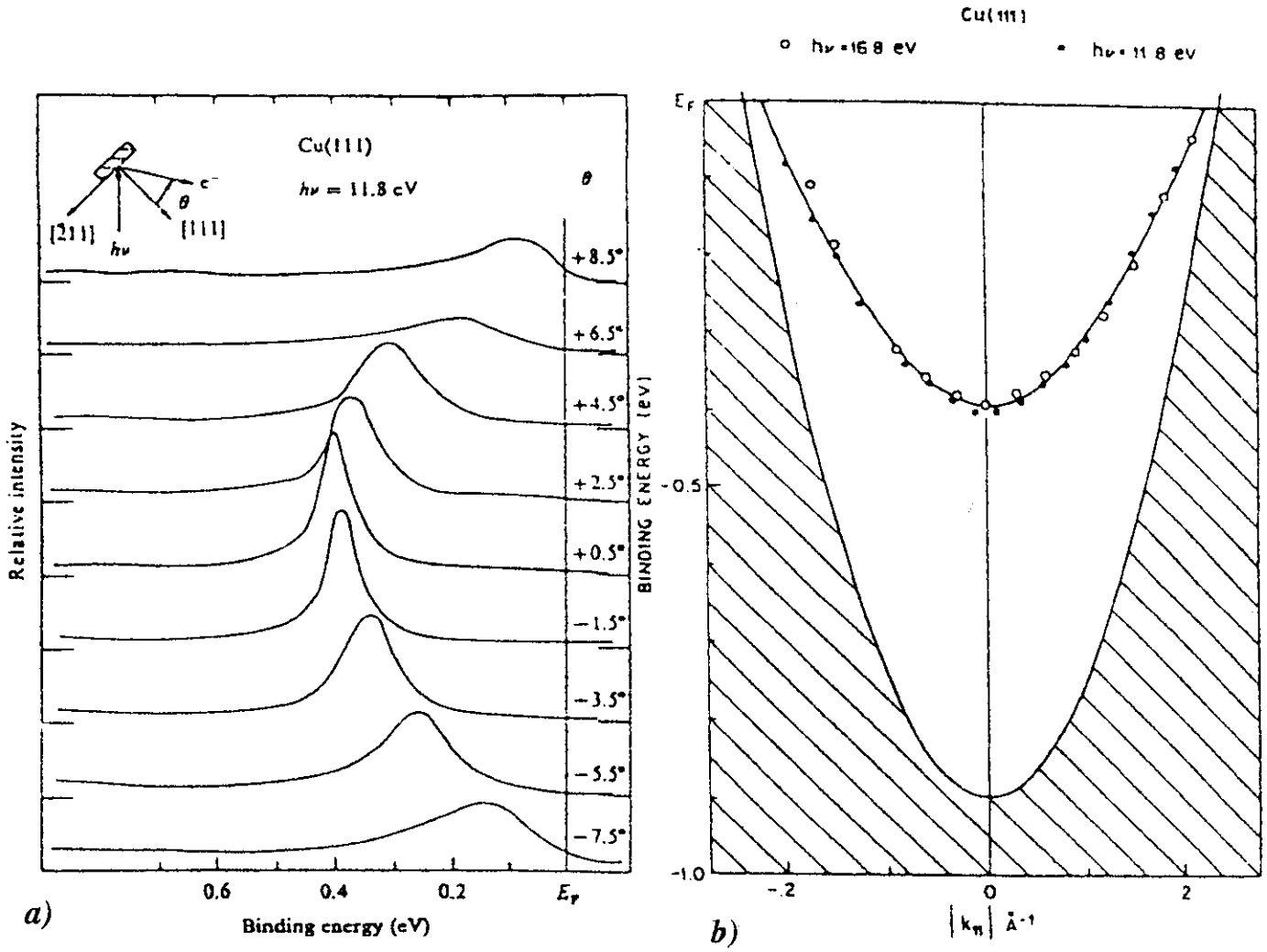

Fig. *5 a) Angular dependent spectra of a sp-surface state at the Cu(111) surface. b) Energy dispersion of the surface state. The shadowed areas indicate the energy regions allowed for bulk states.*

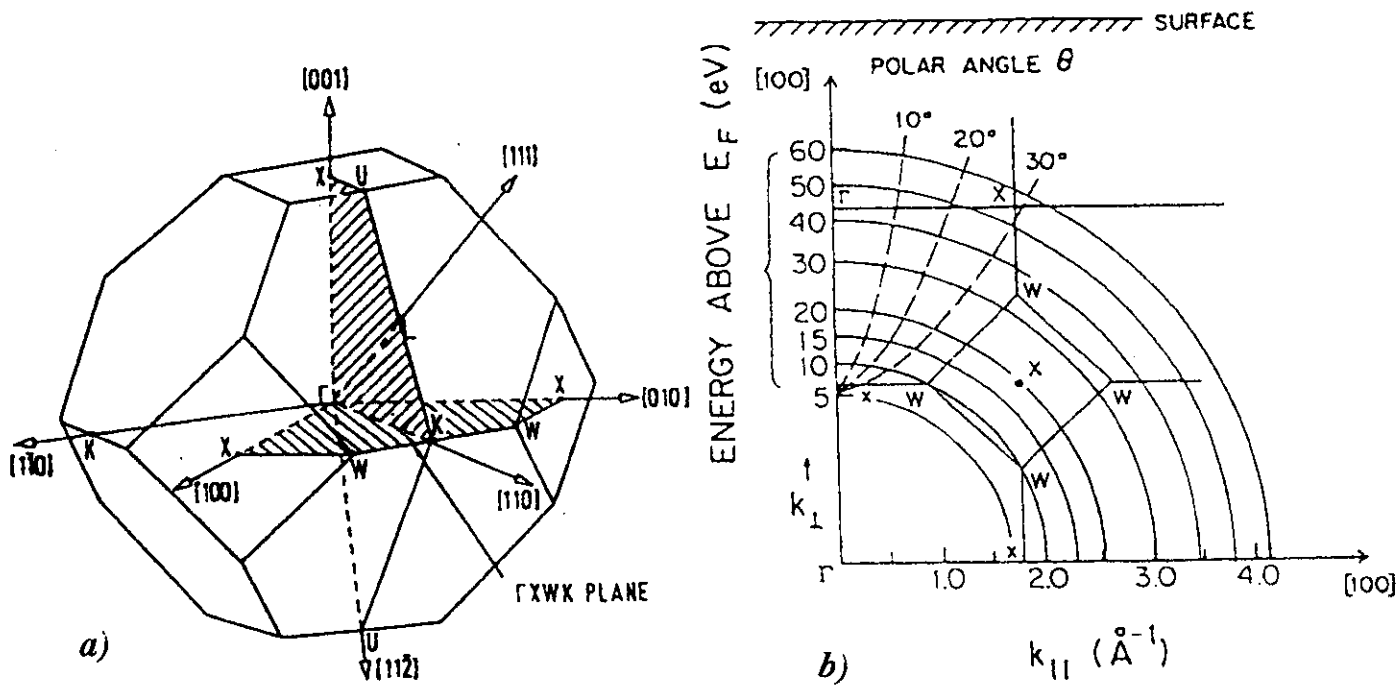

Fig. 5 a) Angular dependent spectra of a sp-surface state at the Cu(111) surface. b) Energy dispersion of the surface state. The shadowed areas indicate the energy regions allowed for bulk states.

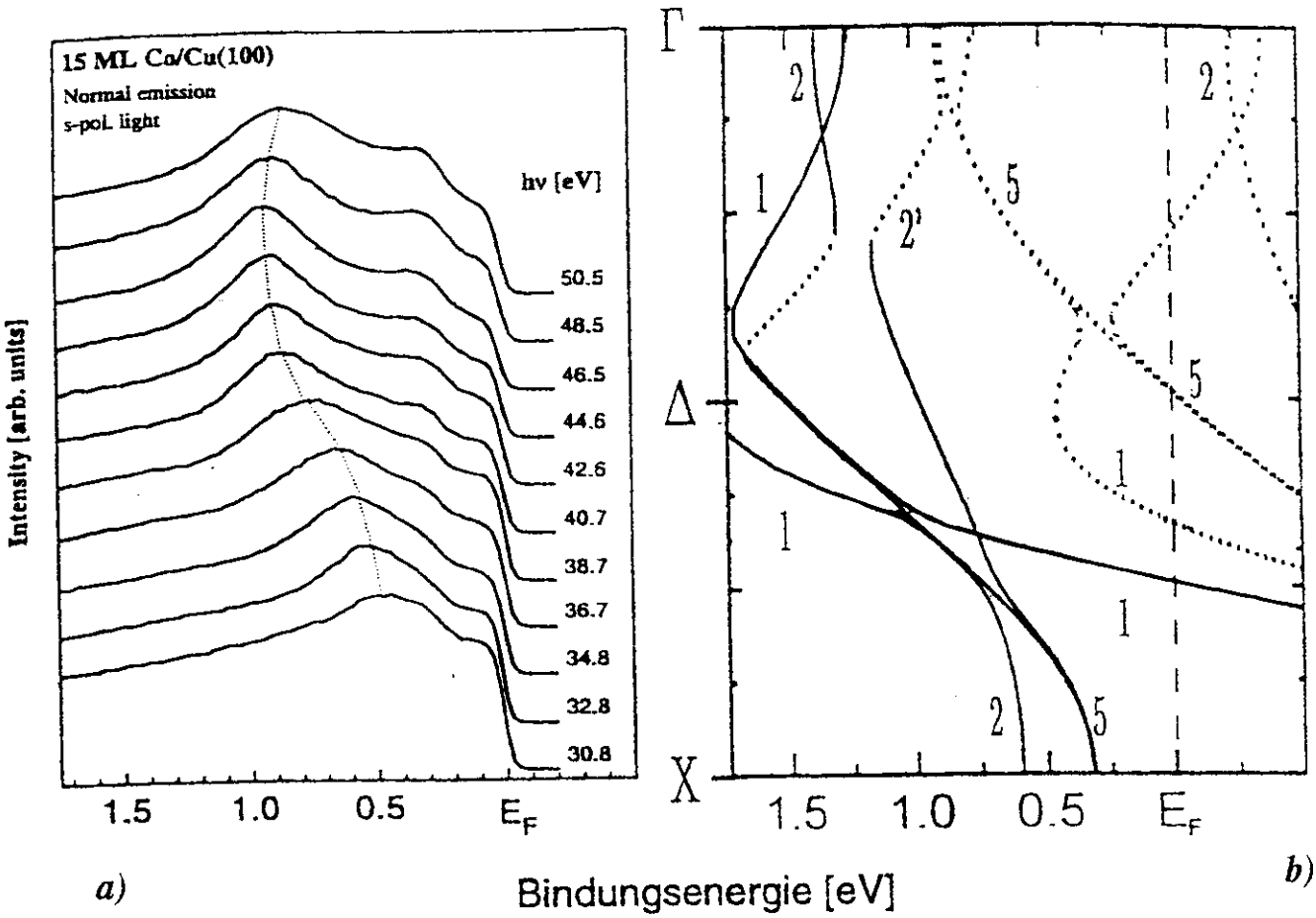

Fig. *7 a) Photoemission of a fcc-Co film (15 atomic layers) on Cu(100) for different photon energy. b) Theoretical (relativistic) bandstructure of fcc-Co along the Γ-X direction.*

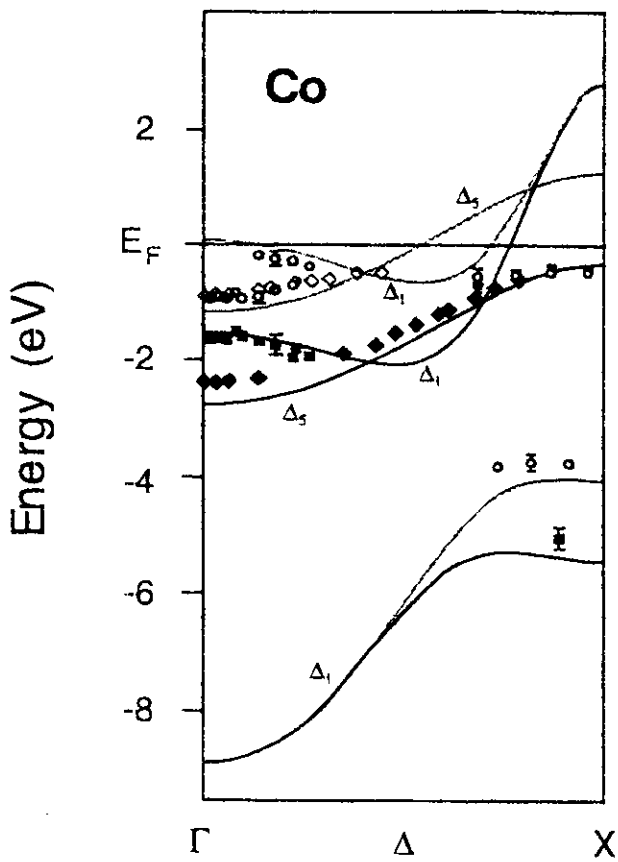

Fig. 10 *Band structure of fcc-Co films. The symbols indicate the binding energy of majority- and minority-spin states (filled and empty symbols, respectively), determined by photoemission experiments. The results of spin-polarized electronic bandstructure calculation are also shown (dark lines: majority-spin bands, light lines: minority-spin bands).*

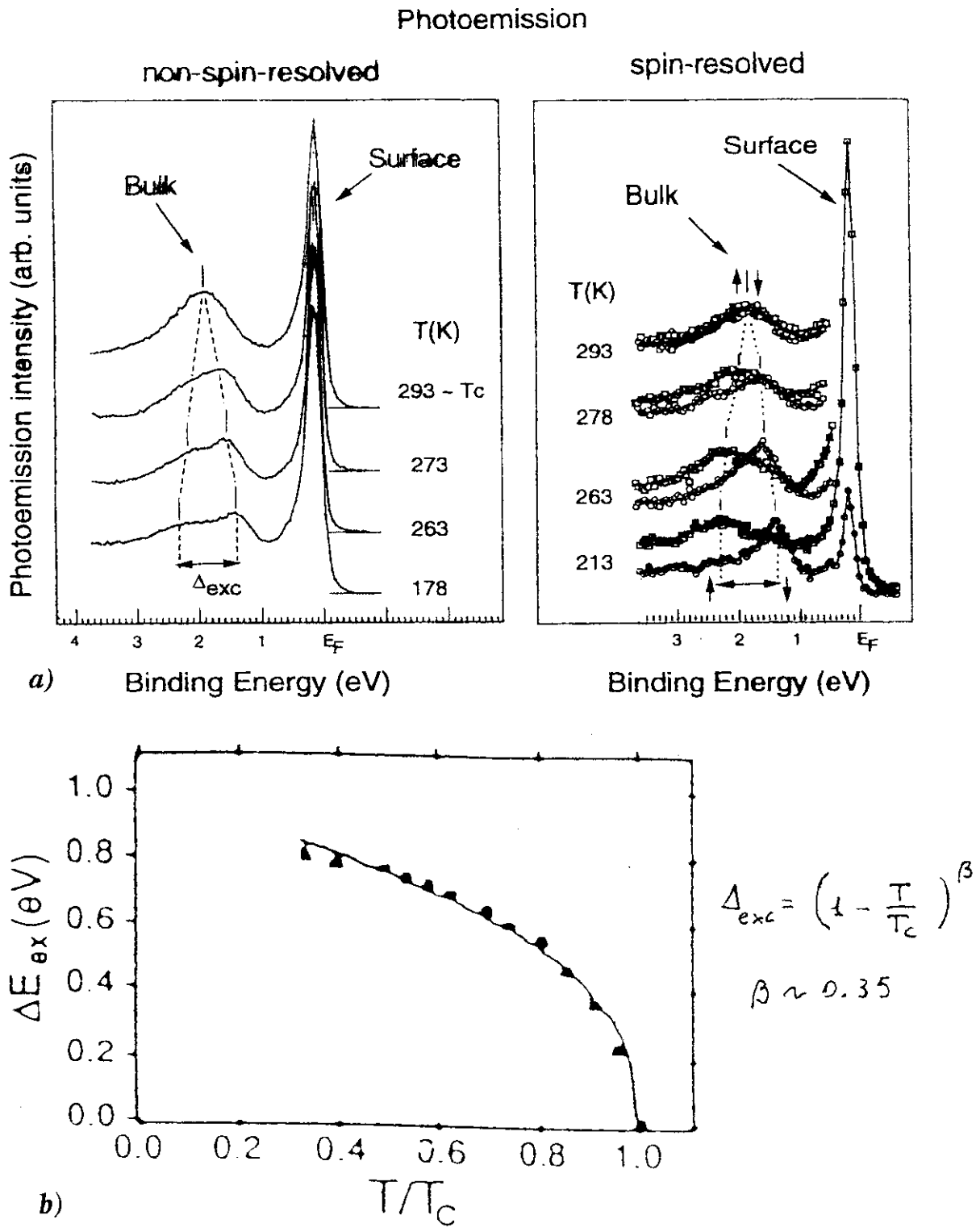

Fig. 11 *a) Spin-integrated (left) and spin-resolved spectra (right) of the Gd valence band. A pair of exchang-split bulk states is observed between 1 and 3 eV binding energy. A majority-spin surface state gives rise an intense emission peak near the Fermi energy. The exchange-splitting of the bulk states decreases with increasing temperature. b) Exchange splitting of Gd bulk states as a function of temperature*

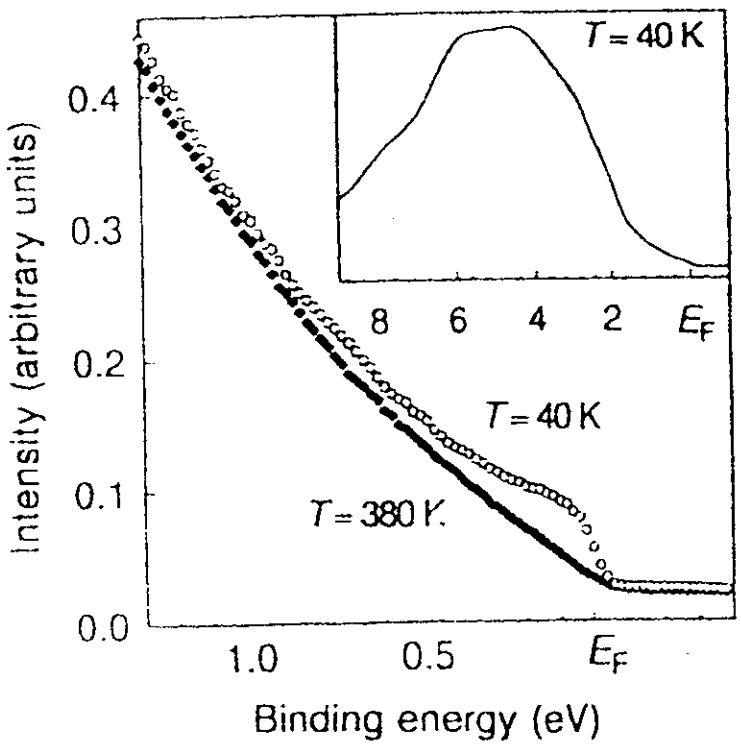

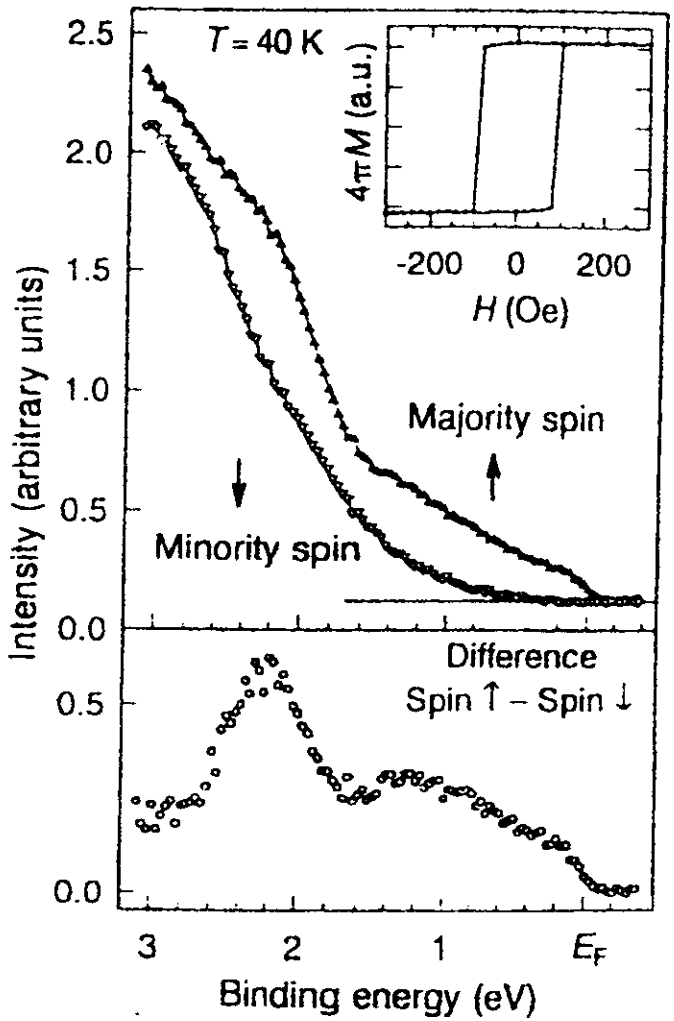

Fig. 12 *Left: Photoemission spectra of a $La_{0.7}Sr_{0.3}MnO$ film near the Fermi energy. The measurements are taken above (380 K) and below (40 K) the Curie temperature (T= 350 K). The inset shows a wide-scan valence spectrum. Right: Spin-resolved photoemission spectra (upwards triangles: majority-spin emission, downwards triangle: minority spin emission) of a $La_{0.7}Sr_{0.3}MnO$ film measured at 40 K, and their difference. The inset shows the film magnetic hysteresis curve.*

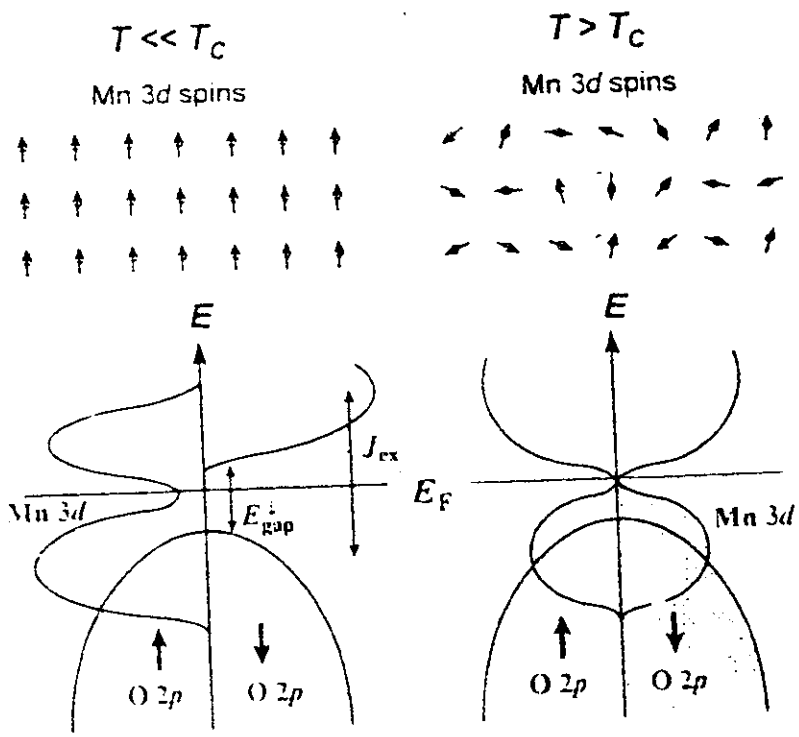

Fig. 13 *Schematic energy diagram and the Mn 3d spin alignements in the* $La_{0.7}Sr_{0.3}MnO$ *film below and above the Curie temperature.*

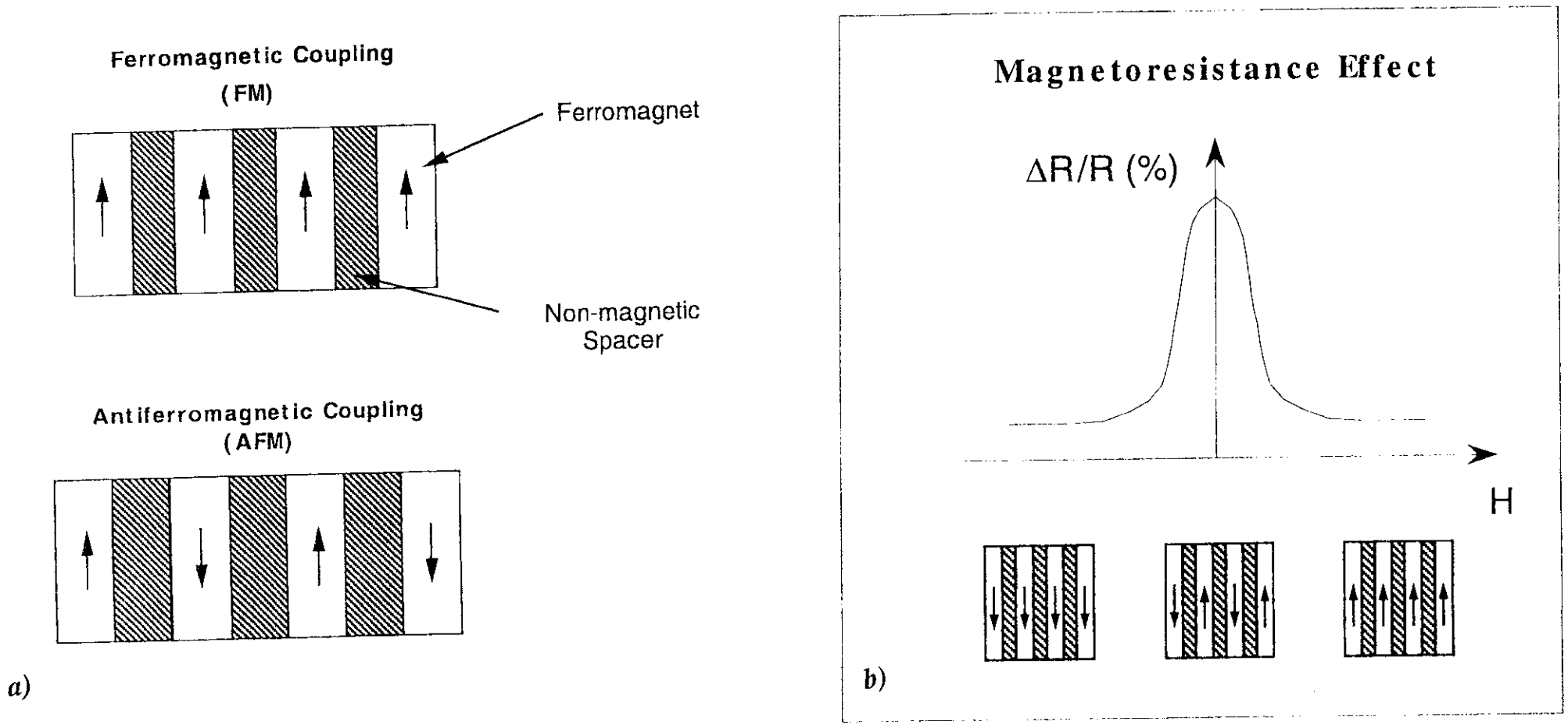

Fig. 14 *a) Schematic representation of the oscillatory coupling between ferromagnetic films separated by a non-magnetic layer. Alternatively parallel and antiparalllel alignement of the film magnetization is obtained by varying the non-magnetic layer thickness. b) Antiparallel coupled film systems display a decrease of the electrical resistance in an external field (GMR effect).*

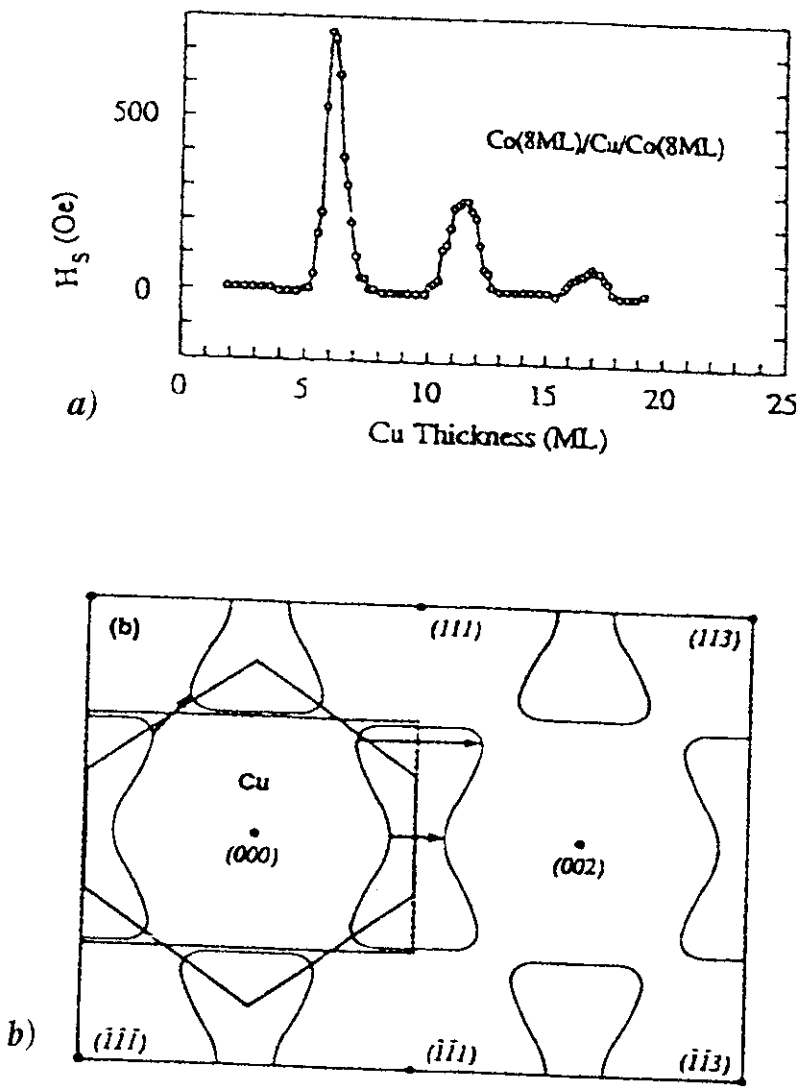

Fig. 15 *a) Magneto-optical Kerr measurement on the oscillatory (~5.9 atomic layer period) behaviour of the coupling of Co films separated by Cu layers. The maxima of the curve correspond to antiparallel coupling, the minima to parallel coupling. b) Extremal spanning vectors across the Cu Fermi surface, that are associated to the two periods (~5.9 and 2.5 atomic layers) of the oscillatiory magnetic coupling through Cu(100) films [22]. The shortest period (2.5 atomic layers) is experimentally observed only on very smooth films.*

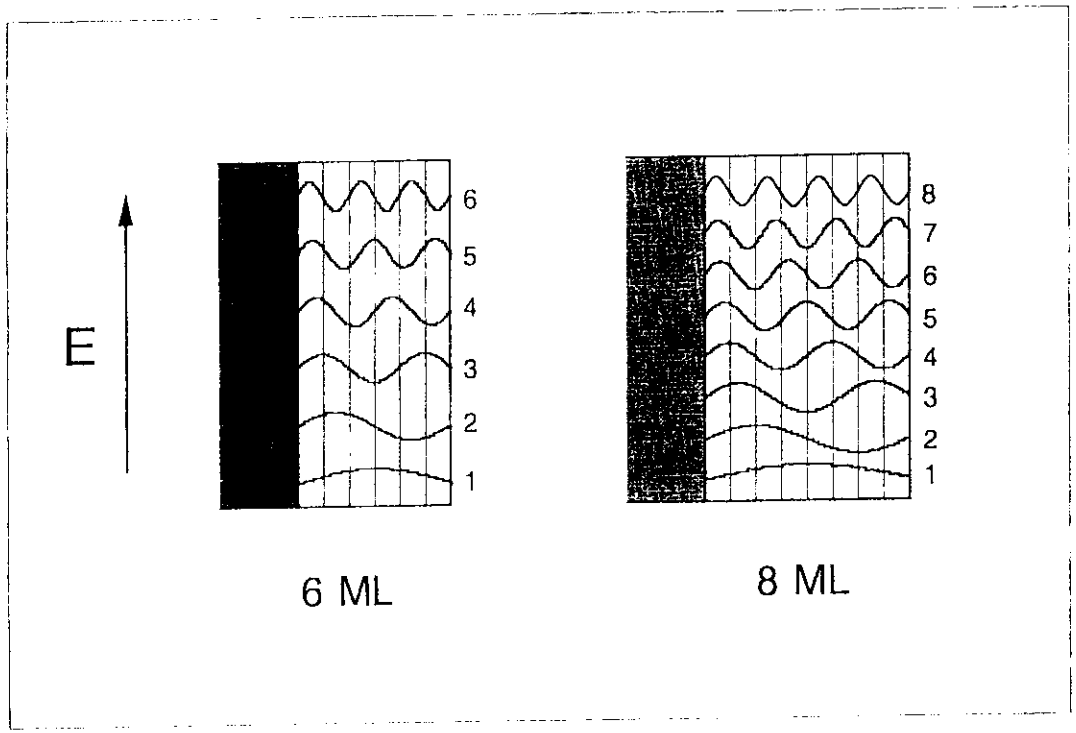

a)

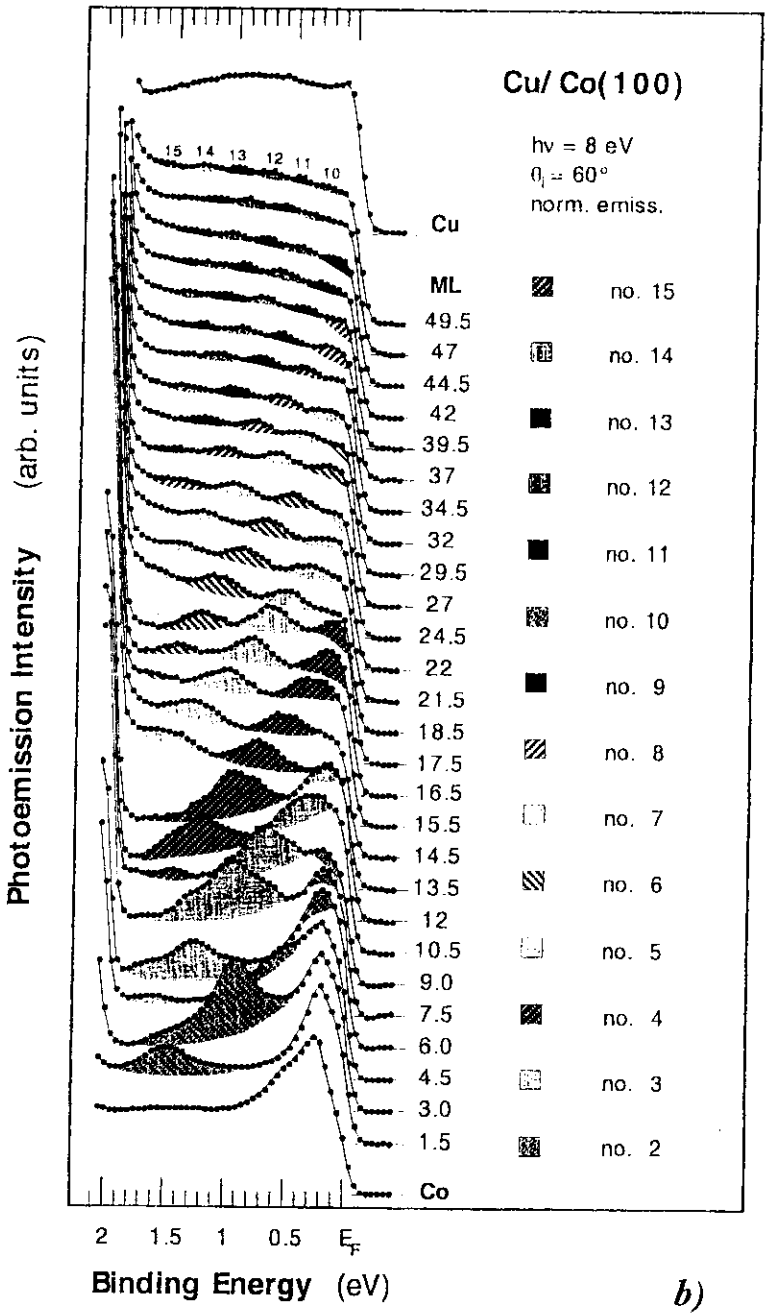

b)

'ig. 16 a) A simple representation of the electronic states of a thin film in analogy to quantum ,ell states. b) Photoemission spectra of ultrathin Cu films on fcc-Co(100). The shadowed pectral structures, with binding energy depending on the film thickness, derive from quanum ,ell states. They are observed up to 50 atomic layers (90 Å) thickn·ss.

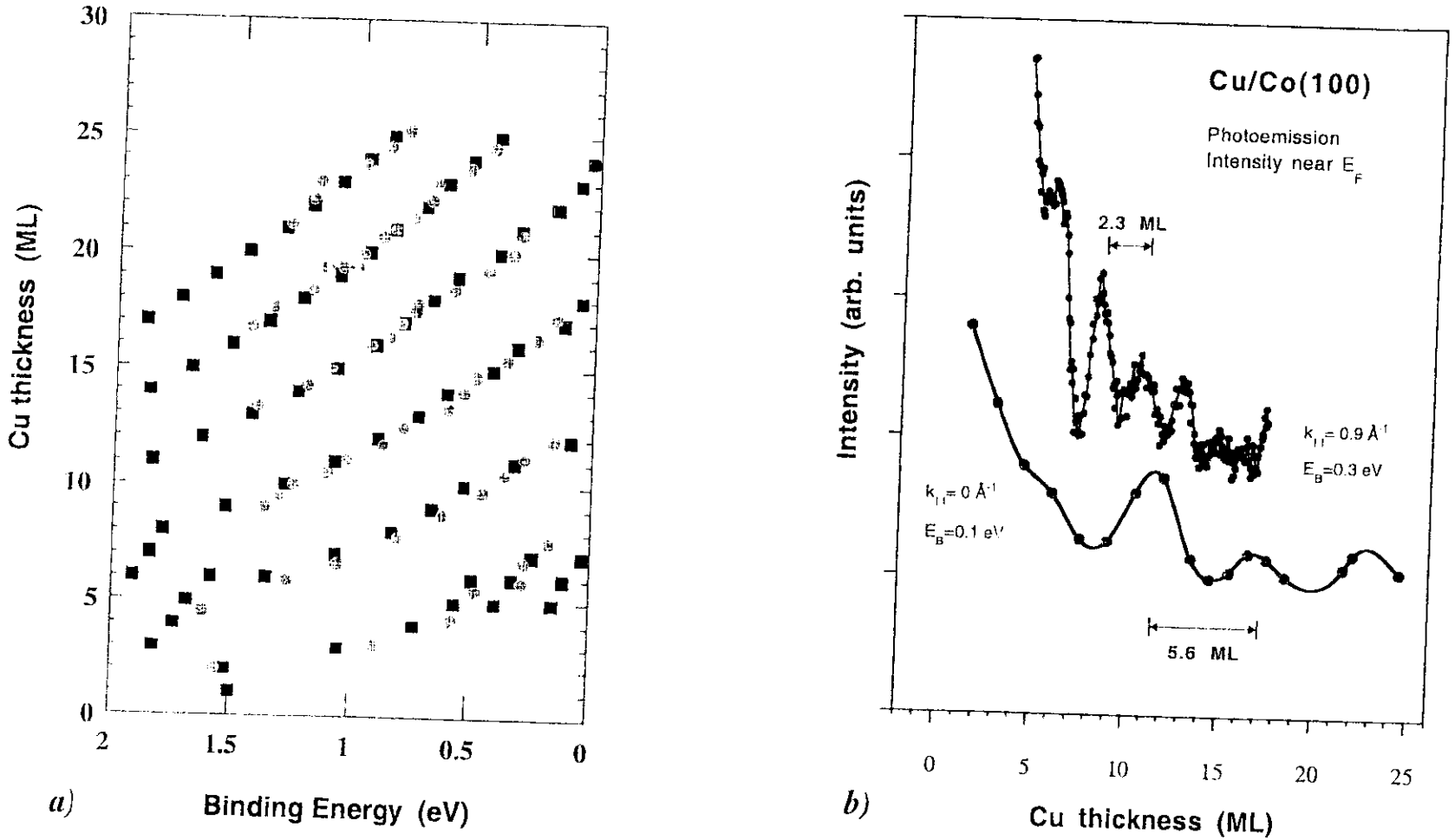

Fig. 17 a) Binding energy of the quantum well states as a function of the Cu film thickness. Circles: experimental data. Squares: theoretical data. b) Oscillations of the photoemission intensity as a function of the Cu film thickness at the two $k_{//}$ point associated to the periods of the oscillatory coupling through Cu(100).

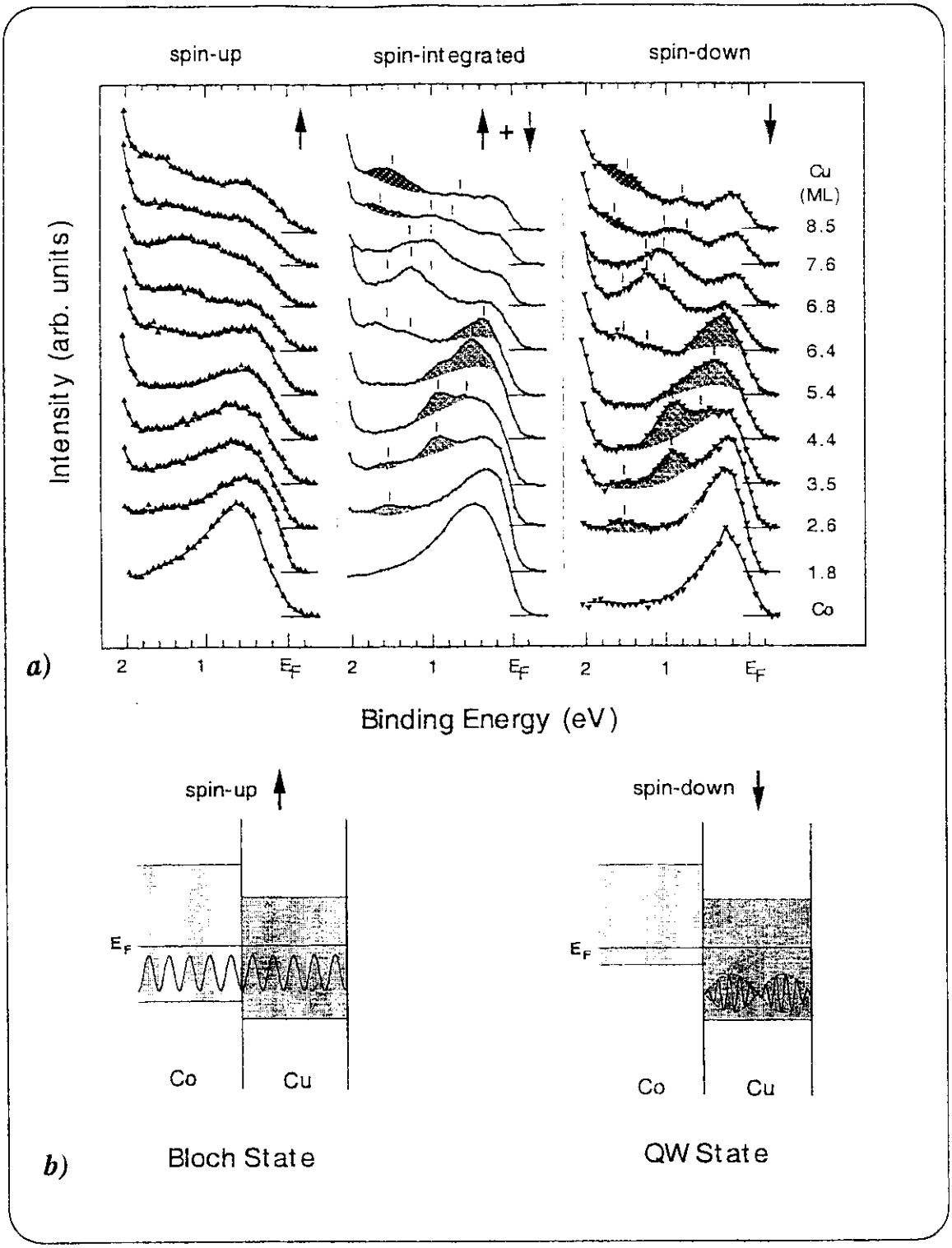

Fig. 18 *a) The photoemission spectrum ($\downarrow+\uparrow$) of thin Cu films on fcc-Co(100) is decomposed into the two spin component, minority ($\downarrow$) and majority ($\uparrow$), by the measurement of the photoelectron spin-polarization. The quantum well states have predominantly minority-spin character. b) The magnetic substrate acts as spin-dependent potential barrier and confines to a different degree the electronic wave function of opposite spin.*

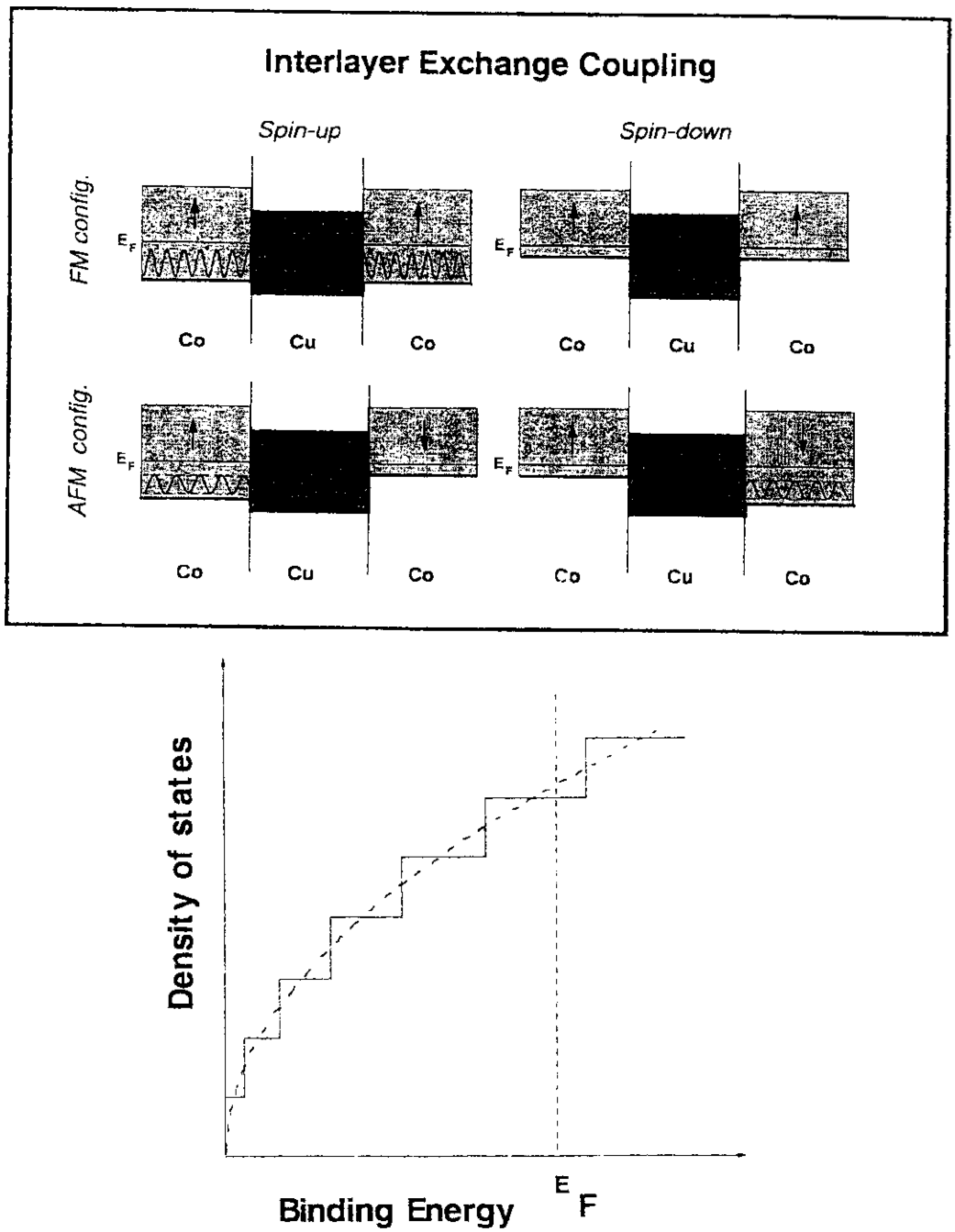

Fig. 19 *Left: Scheme of the quantum well potential (black solid lines) for two magnetic films (Co) separated by a non-magnetic layer (Cu). The top-left (-right) panel represents the potential felt by a spin-up (-down) electron for parallel alignement of the two film magnetization. The bottom-left (-right) panel indicates the potential for a spin-up (-down) electron for antiparallel alignement. Quantum well states are formed by spin-down electrons only for parallel alignment of the film magnetization. Right : Density of states for electrons confined in the film (solid curve) and for a free electron (dashed curve). The corresponding energy difference determine the sign of the interlayer coupling.*

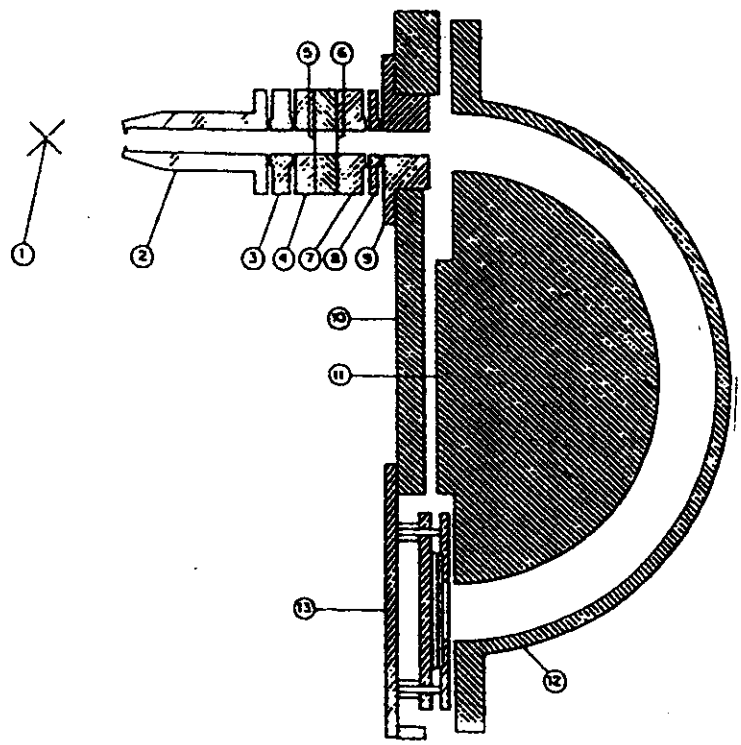

Fig. 20 *Scheme of an electron energy analyzer: (1) sample), (2-9) electron optics, (11-12) inner and outer half-sphere, (13) two-dimensional detector*

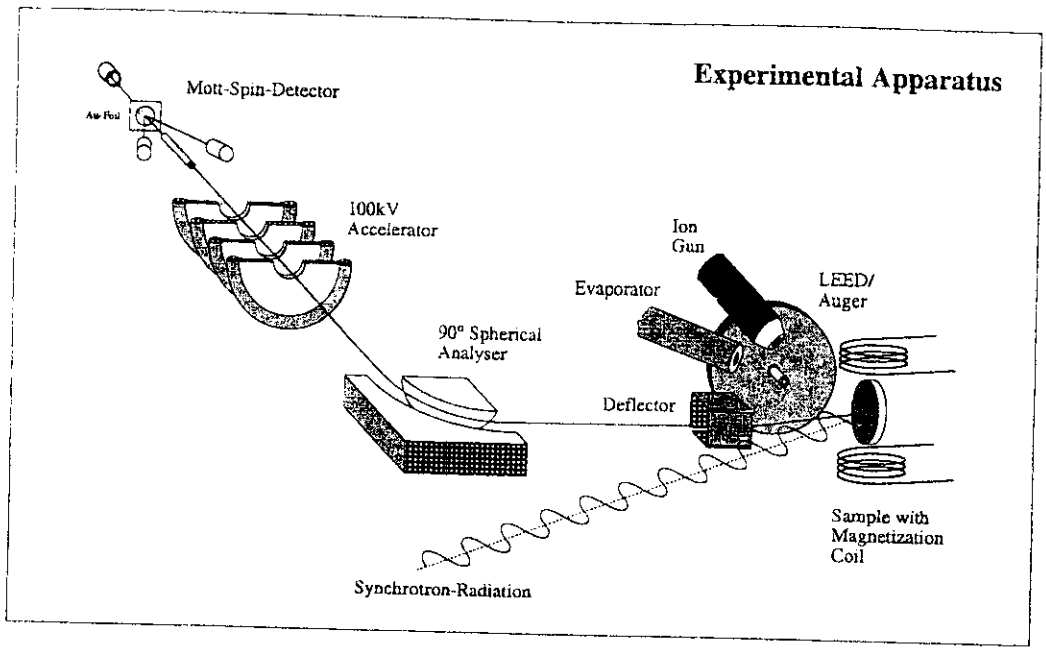

Fig. 21 *Diagram of an experimental apparatus for spin and angle resolved photoemission. Electron energy and momentum are determined with a dispersive electrostatic analyzer coupled to a spin-detector for the measurement of the photoelectron spin polarization.*